Fast solitary waves against slow inertial instability in stimulated Raman scattering

Antonio Picozzi, Carlos Montes,* and Eric Picholle
Laboratoire de Physique de la Matière Condensée, Centre National de la Recherche Scientifique, Université de Nice–Sophia Antipolis, Parc Valrose, F-06108 Nice Cedex 2, France
(Received 5 March 1998)

We investigate the dynamics of the backward stimulated Raman process in optical fibers; the spatiotemporal (1+1)-dimensional three-wave dissipative inertial model accounts for the noninstantaneous Raman response of the medium, the optical Kerr effect, and the group velocity dispersion. A different class of dissipative superluminous solitary structures emerges from a chaotic Stokes dynamics. In contrast with the nonlinear Schrödinger class of equations, the velocity of the solitary wave plays a key role and has been determined by the Kolmogorov-Petrovskii-Piskunov procedure. The long-term evolution of the three-wave resonant interaction is ruled by two competing instabilities: the convective Raman instability, characterized by the velocity of the leading front, and an ''inertial instability,'' which arises through the combined actions of the Kerr effect and the noninstantaneous response of the medium. By comparing their relative growth rates we find a criterion that determines the asymptotic pattern selected by the system (solitonlike or chaotic) and give relevant experimental parameters. [S1063-651X(98)02408-8]

PACS number(s): 42.65.Tg, 42.65.Dr, 42.81.Dp, 42.65.Sf

I. INTRODUCTION

During the past two decades, the intense research activity in the field of nonlinear fiber optics has resulted in a number of breakthroughs that revolutionized the communications capabilities. However, many fundamental aspects of nonlinear interactions of light with matter are still poorly understood. Of particular interest is the resonant coupling between an optical field and the natural oscillation modes of its propagation medium, which naturally yields both nonlinear and noninstantaneous responses. The stimulated Raman scattering (SRS) process is a typical example of resonant light-matter interaction.

In optical fibers, SRS exhibits a particularly complex dynamics, mainly because it is accompanied by the optical Kerr effect, always of the same order of magnitude, and the group velocity dispersion [1,2]. Simplified models have thus been introduced in a preliminary approach of regular temporal pattern formation. We can distinguish three main themes among the vast Raman literature.

(i) In the context of short pulse propagation in optical fibers, SRS was first considered as a perturbation to the optical Kerr effect and group velocity dispersion. Its modeling then calls for a perturbed nonlinear Schrödinger (NLS) equation, which allows an improved description of intrapulse Raman scattering, including the self-frequency shift observed during optical soliton propagation [3,4]. Stationary shock-wave solutions have been exhibited in both the normal (positive) [5,6] and anomalous (negative) dispersion regimes [7,8].

(ii) In SRS lasers or amplifiers, two optical components are spectrally distinguishable, namely, the pump and its scattered Stokes wave. The problem is more complicated and is usually described through two coupled NLS equations accounting for the Raman process but assuming the material excitation to respond instantaneously; we will refer to this as the ''standard model'' of SRS in optical fibers [9]. A family of shock-wave solutions of the dispersionless problem has been identified [10] and an analytical bright-dark solitary-wave pair solution has even been exhibited in the full problem (SRS, Kerr effect, and dispersion) [11].

(iii) In gases, the optical Kerr effect and the dispersion can usually be neglected. On the other hand, the response time of the medium, typically in the picosecond range, is comparable to the characteristic evolution time of the optical envelopes and the dynamics of the vibrational modes must be taken into account. Their noninstantaneous response is described through an additional equation for the material excitation, besides the two equations for the optical waves. In this pure three-wave resonant model the laser pump stimulates the scattered Stokes wave through the material excitation [12,13]. Transient SRS was considered in this context [14] and three-wave soliton behavior has been predicted [15] and subsequently observed [16]. Moreover, the three-wave resonant interaction in presence of dispersion (or diffraction) is of particular interest at present in nondegenerate parametric interactions [17].

The purpose of this paper is to investigate the solitary-wave dynamics of the stimulated Raman backscattering process in the frame of a more general ''inertial model'' accounting for the noninstantaneous Raman response, the optical Kerr effect, and the group velocity dispersion [2]. To a certain extent, this work bridges approaches (ii) and (iii) discussed above. A different class of stable three-wave coherent solitary solutions is presented. Inferring from the well-known NLS-like soliton dynamics [6], one should expect that the *velocity* of the traveling-wave solution would be irrelevant. It is indeed the case for the SRS solitary structures described by the standard model; however, in the inertial model, the three-wave resonant interaction *breaks the existence of the gauge transformation* responsible for this property. The velocity of the solitary wave thus becomes a relevant parameter even in dispersive media. In order to analyze

*Electronic address: montes@unice.fr

its selection mechanism, we extend the Kolmogorov-Petrovskii-Piskunov procedure [18–20], which proved quite powerful in nonlinear diffusion problems [21,22]. These three-wave solitary structures are intrinsically dissipative and proved to be robust with respect to external perturbations; they can be considered as *attractors* in spatially extended media.

We also distinguish the usual convective Raman instability and a different ''inertial instability.'' The former originates in the three-wave coupling and is characterized by the velocity of the leading front (Sec. IV); it can be saturated by the depletion of the pump. The inertial instability, which is analyzed in Sec. V, can avoid the depletion of the pump. It originates in the coupling between the optical Kerr effect and the noninstantaneous material response and thus arises even in the absence of dispersion; this is a major difference from the well-known modulational (Benjamin-Feir) instability, which is intimately related to the group velocity dispersion [9].

The long-term evolution of the three-wave interaction is ruled by the two competing instabilities. When the growth rate of the inertial instability dominates, the interaction evolves asymptotically towards a chaotic dynamics. Otherwise, the system self-structures in a three-wave solitonlike behavior. This self-similar superluminous motion then emerges from the chaotic dynamics, which propagates at the luminous velocity; the velocity of the leading front of a pulse thus governs its whole asymptotic dynamics.

II. INERTIAL MODEL

Considering the nonlinear effects as perturbations to the linear propagation, the optical fields can be described as weakly interacting wave packets through the slowly varying envelope approximation. The equations governing the evolution of the optical fields are derived following a usual approach that leads to NLS-like equations [9] and takes into account the Kerr effect and the group velocity dispersion. Since the material response time is very short (about 75 fs in silica), it is neglected in most models of stimulated Raman scattering in fibers as the typical pulse width lies in the picosecond range and above. Most recently, more complete models have underlined the relevance of the noninstantaneity of the medium response when the pump and Stokes waves can be distinguished [1]. We have discussed this approximation in a previous work and shown that this nonlinear inertial response can dominate the linear group velocity dispersion even in the picosecond regime for strong enough pump powers (typically several watts) [2]. In polarization-maintaining single-mode fibers, effective parameters account for the full space-time dynamics of SRS through this one-dimensional inertial model, which describes the Raman process through a resonant interaction between the optical fields and the natural vibrational modes of the medium. An additional equation describes the excitation of a collection of harmonic oscillators coherently driven by the applied optical field [23,4].

While most previous studies dealt with forward SRS, we will consider the backward configuration also of interest for SRS's sister interaction, namely, the stimulated Brillouin scattering (SBS) for which earlier studies have revealed a rich nonlinear dynamics, including spatiotemporal chaos [24] as well as solitonic behaviors [25,26]. We are interested here in the resonant case, where the SRS process couples a pump $E_p(\omega_p,k_p)$ and its backscattered Stokes wave $E_S(\omega_S,k_S)$ to a material response $E_a(\omega_a=\omega_p-\omega_S,k_a=k_p+k_S)$ proportional to the molecular polarization and with the dimension of an electric field. The three coupled equations thus read in dimensionless units

$$(\partial_t+\partial_x+i\rho\partial_{tt}+\mu_p)E_p=-E_SE_a+i\kappa[|E_p|^2+2|E_S|^2]E_p, \tag{1a}$$

$$(\partial_t-\partial_x+i\rho\partial_{tt}+\mu_S)E_S=E_pE_a^*+i\kappa[|E_S|^2+2|E_p|^2]E_S, \tag{1b}$$

$$[(1+2i\alpha\mu_a)\partial_t+\mu_a]E_a=E_pE_S^*, \tag{1c}$$

where the complex envelope amplitudes $E_i=|E_i|e^{i\phi}$ and the time t, space x, and damping rate γ_i are normalized to the constant pump input $E_0=|E_{cw}|$ and to the SRS coupling constant K ($=509\ \mathrm{m\,sec^{-1}\,V^{-1}}$ in silica fibers) [$E_i/E_0\rightarrow E_i$, $tKE_0\rightarrow t$, $xcKE_0/n\rightarrow x$, and $\gamma_i(KE_0)^{-1}\rightarrow\mu_i$ ($i=p,S,a$)]. n is the linear refractive index (effective index $n\cong1.46$) and the Kerr parameter $\kappa=n_2\omega_pE_0/2nK$ is proportional to the nonlinear refractive coefficient n_2 ($=1.22\times10^{-22}\ \mathrm{m^2/V^2}$). The dispersion parameter is $\rho=k''KE_0c/2n$, where $k''=\partial^2k/\partial\omega^2$, and finally $\alpha=(KE_0/2\omega_a)$ appears as a detuning parameter. We also define the phase mismatch $\Phi=\phi_p-(\phi_S+\phi_a)$ (Appendix A). The nonlinear Raman and Kerr processes can be quantitatively compared in steady regimes [or in the frame of the standard model, obtained through the adiabatic approximation of Eq. (1c)] by replacing in Eqs. (1a) and (1b) the expression $E_a=E_pE_S^*/\mu_a$; in fibers, they are always of the same order since $\kappa\mu_a\cong4$ (whereas $\kappa\mu_a\cong10^{-2}$ and the dispersion can be neglected in the SBS case).

In very long (semi-infinite) media, a constant pump level is necessary to compensate for the optical and material dampings, but can be achieved in a simple configuration only if one neglects the damping of the pump wave. We will thus make this approximation ($\mu_p=0$) which is locally legitimate as long as the interaction times (practically, the width of the considered structures) are small compared to μ_p^{-1}, a condition always verified in low loss optical fibers.

III. NUMERICAL THREE-WAVE DYNAMICS

One cannot exhibit explicit analytical solutions of system (1) since the dissipative three-wave model is not integrable [27]. Before looking for an alternative theoretical analysis, let us first investigate numerically, in the frame of the inertial model and for various initial conditions, the existence and robustness of solitary-wave solutions. In this paper, for the sake of simplicity, we will discuss only the normal dispersion regime, in which no solitary solutions have been exhibited in the frame of the standard model of SRS. Our basic problem, of particular interest for amplification devices, is the propagation of an initial localized Stokes pulse [$E_S=\mathrm{sech}(kx)$] with wave-front slope k, in the presence of a counterpropagating continuous pump.

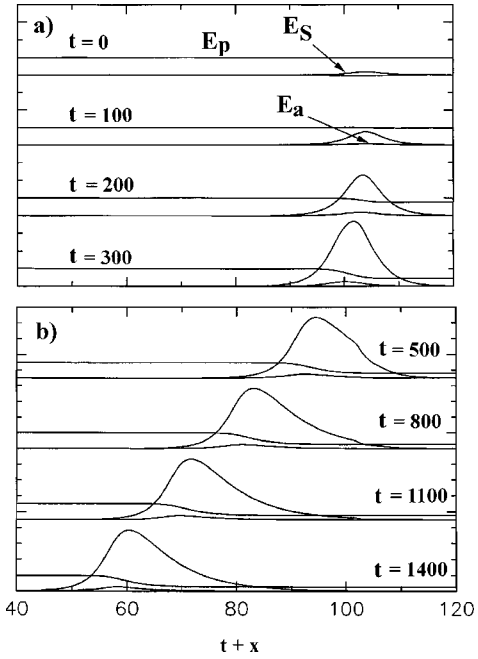

FIG. 1. Self-structuring of a three-wave solitary solution [numerical computation of Eqs. (1) ($k=0.35$) in the luminous Stokes reference frame]: (a) transient amplification stage and (b) asymmetric solitary structure, whose superluminous velocity is associated with the drift towards the left of the luminous window (for better visibility, E_a has been magnified $5\times$).

A. Solitary-wave self-structuring

We solve numerically Eqs. (1) by following the characteristics in the comoving Stokes frame [26], the optical dispersion being obtained by a five-point finite difference scheme [27]. In Fig. 1 we plot the typical evolution in the normal dispersion regime ($k''=1\ \mathrm{ps}^2/\mathrm{km}$) of a sechant Stokes shape of slope $k=0.35$, which corresponds to a 25-ps pulse for a peak amplitude $E_S=10$ MV/m and the same continuous pump level. During the first stage of the interaction ($t<100$), the Stokes field and the material excitation are amplified in the parametric regime, here defined by a nearly constant pump wave [$E_p(x,t)=1$]. In a second time the total energy of the Stokes and material fields becomes sufficient to deplete the pump ($t>200$). The backward configuration breaks the $t\rightarrow -t$ symmetry of the problem and gives rise to an asymmetric amplification process: The leading edge of the pulse follows a strong amplification to the detriment of the trailing edge where the pump is depleted, yielding superluminous Stokes and material fronts. In the long-term evolution, the system self-structures in a superluminous three-wave solitary structure of constant width. This superluminous solitary motion can be viewed as the result of the convective amplification of the leading edge of the Stokes and material pulses, whereas their rears are attenuated [25]; no information can be transported via this *pulse reshaping process* [28]. Figure 2 describes the evolution of a narrow structure artificially superimposed on the solitary solution; in the (luminous) reference frame of the Stokes energy, we observe the separation of a stationary localized defect that propagates at the luminous velocity from the solitary wave drifting away with its superluminous velocity. The solitary structure and the defect behave as two independent

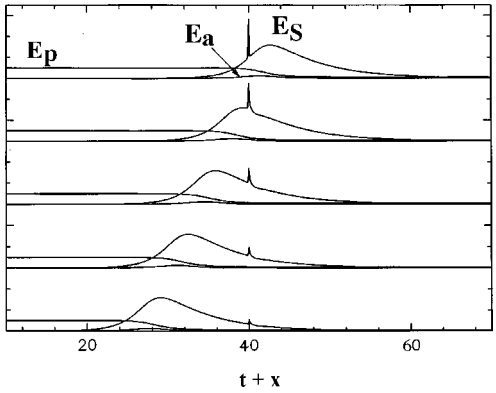

FIG. 2. Evolution of a defect artificially superimposed onto the solitary wave. The luminous localized defect slides on the superluminous tail of the solitary structure.

objects, the former being asymptotically stable and the latter rapidly damped, since the depleted pump is insufficient to compensate for the losses in the trailing edge. As in the SBS case, this decoupled evolution strongly contributes to the robustness of these dissipative solitary structures [29].

The solitary solution presented here is valid in the normal dispersion regime and is thus completely different in nature from the solution exhibited in the frame of the standard model [11]. The latter still depends on a Kerr-dispersion balance, characteristic of the NLS-based equations, while the SRS compensates for the losses: the Stokes and pump wave must have bright and dark soliton profiles and propagate, respectively, in the anomalous and normal dispersion regimes. On the other hand, the present solution is closer to the regular three-wave solitons observed in gases [16], even if the dissipation is strong and the intensity profiles are affected by a complicated phase dynamics induced by the Kerr and dispersion effects (while the pure three-wave resonant interaction involves only real amplitudes [13,26]).

The solution in Ref. [11] is characterized by a full reconstruction of the pump (hyperbolic tangent), which is thus able to destabilize the far tail of the Stokes pulse. This is not the case here: The solitary-wave trajectory in the phase space links an *unstable* fixed point (far leading front: $|E_p|=1$, $E_S=E_a=0$) to a fix point with a pump power below threshold (far pulse tail: $|E_p|\cong 0$, $E_S=E_a=0$) and thus is always *stable*. Locally, the passage of the solitary wave can be described as the *transition* of the system toward a stable state, which again emphasizes its robustness.

Let us note the strong asymmetry of the Stokes envelope that characterizes the dissipative nature of the solitary-wave solution [30]. In fact, the dissipation is intrinsically related to the noninstantaneous response of the medium, as can be seen in Eq. (1c), where μ_a^{-1} represents the lifetime of the material excitation. A specific invariant characterizes the solitary motion. We show in Appendix B that the pulse energy of the Stokes and material fields, defined as $W_{S,a}=\int_{-\infty}^{+\infty}|E_{S,a}|^2 d\tau$, satisfy the relationship

$$\partial_\xi W_S = 2\mu_a W_a - 2\mu_S W_S + 4i\alpha\mu_a \int_{-\infty}^{+\infty} E_\alpha^* \partial_\tau E_a d\tau, \quad (2)$$

where $\xi=-x$ and $\tau=t+x$ are retarded variables. Due to their conservative nature, the optical Kerr and dispersive ef-

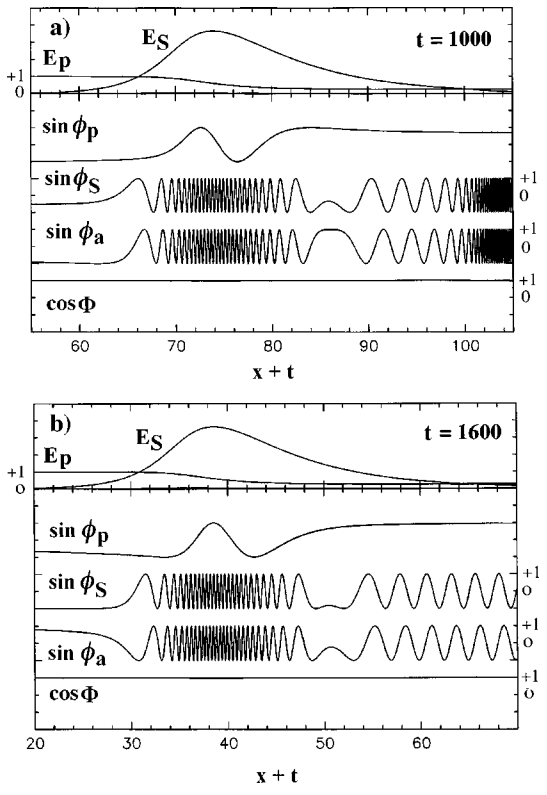

FIG. 3. Profiles of the modulus $|E_{p,S}|$ and phases sin $\phi_{p,S,a}$ in the solitary regime for (a) $t=1000$ and (b) $t=1600$. The three phases follow a complex dynamics, but the phase mismatch cos Φ remains constant.

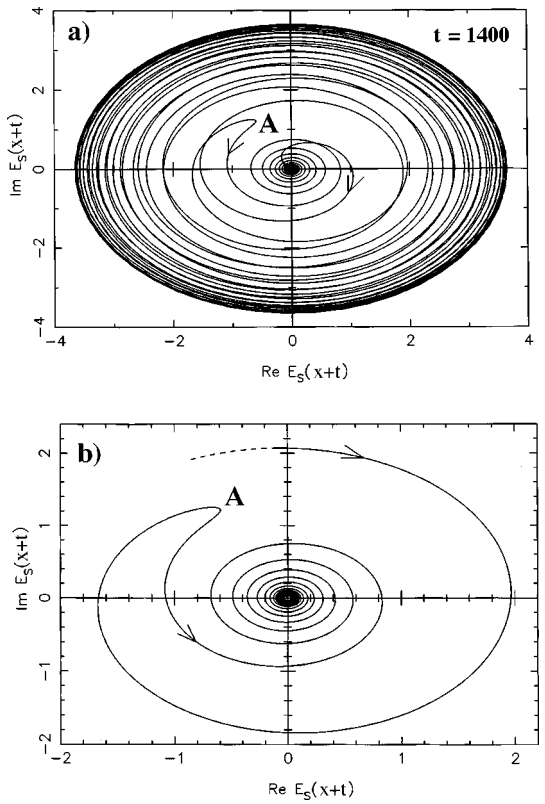

FIG. 4. (a) Phase portrait of the complex Stokes field in the solitary regime ($t=1400$). The rotation of the phase is inverted at point *A*. (b) A zoom of *A*.

fects do not play any role in this relation. A solitary-wave behavior calls for the three fields to be in their asymptotic steady state, thus $\partial_\xi W_S=0$ and Eq. (2) yields the expression of the invariant; it has been used as a criterion for the asymptotic nature of the solitary solutions and to check the accuracy of the numerical scheme.

Phase dynamics of the solitary wave

We plot in Fig. 3 the profiles of the modulus $|E_{p,S}|$ of the optical fields and their respective phases $\phi_{p,S,a}$ in the asymptotic solitary regime for two values of the interaction time. The key parameter characterizing the coherence of the three-wave interaction is the phase mismatch Φ. The simulations show that, despite the complex (but fairly complementary) phase structure of the Stokes and the material fields, Φ remains almost constant over the whole interaction range. It is worth noting that this classical feature of the pure three-wave resonant interaction is still valid in the presence of optical Kerr and dispersion effects, despite the fast rotation of the phases they induce (Appendix A). Between $t=1000$ [Fig. 3(a)] and $t=1600$ [Fig. 3(b)], the three moduli remain unchanged, but the phases evolve rapidly. The concept of attractor is strongly related to the dissipative nature of the interaction and thus is valid only as far as the modulus is concerned. The apparent Stokes frequency is stable in the body of the pulse, but rapidly evolves in its trailing edge. We plot in Fig. 4 the phase portrait of the Stokes field in its own reference frame [Re E_S, Im E_S] at time $t=1400$. The rotation of the Stokes phase is inverted on a particular point *A* of the solitary wave. This complex dynamics contrasts with the smooth phases characteristic of NLS like solutions.

B. Solitary-wave emersion from chaotic dynamics

For shorter pulses the three-wave interaction becomes incoherent and is no longer able to keep Φ constant. We plot in Fig. 5 the evolution of a secant Stokes pulse ten times narrower than in the previous case. The asymptotic evolution of the Stokes wave packet is completely different. The amplification of the Stokes wave is accompanied by an asymmetric distortion that evolves asymptotically towards an erratic behavior and the overall width of the structure keeps increasing

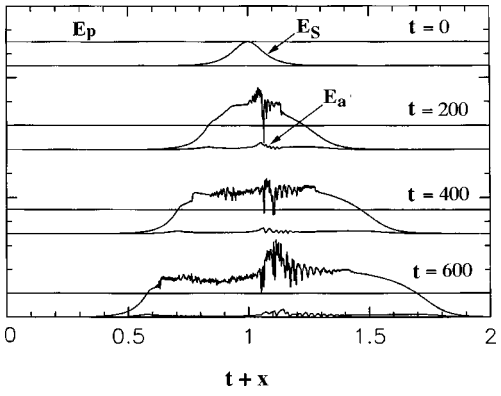

FIG. 5. Same as Fig. 1, but with a ten times narrower Stokes pulse ($k=18$). The inertial instability appears at the peak and yields asymptotically a chaotic behavior, while the pump remains essentially undepleted.

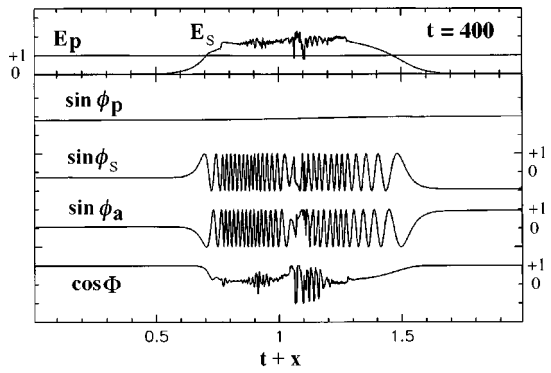

FIG. 6. Profile of $|E_{p,S}|$, $\sin\phi_{p,S,a}$, and $\cos\Phi$ ($t=400$). The three-wave interaction is coherent (incoherent) at the wings (peak) of the pulse.

in time. The chaotic nature of the dynamics has been confirmed in Ref. [2] through the exponential divergence of a perturbed solution from the unperturbed one. Here we focus our attention on the origin of this inertial instability, which becomes dominant at strong pump power and whose creation is directly related to the coupling of the Kerr effect with the noninstantaneous response of the medium, as will be demonstrated in Sec. V through a stability analysis. Unlike the usual modulational (Benjamin-Feir) instability that originates in dispersive Kerr media, *the inertial instability can grow even in the absence of group velocity dispersion.*

Let us remark that in contrast to the previous case analyzed in Fig. 3, the intensity and the phase of the pump field remain almost constant in the whole interaction region ($E_p=1$). This is a consequence of our counterpropagating configuration: The total energy of the Stokes pulse is not sufficient to affect noticeably the pump evolution during the short interaction time, comparable to the pulse width (dispersive walkoff may yield a similar effect for shorter pulses in the copropagative scheme). On the contrary, the dynamics of the Stokes wave and the material excitation is rather complex (Fig. 6, $t=400$). The interaction is coherent at the wings of the Stokes pulse ($\Phi=0$): The phases follow a regular evolution along the propagation. However, with higher Stokes intensity, the peak of the pulse develops the instability that evolves towards a chaotic behavior. In this region $\Phi\neq 0$: The chaotic dynamics *breaks the phase matching* of the three waves; the pump-to-Stokes conversion efficiency can even be averaged to zero, thus avoiding the depletion of the pump. This situation remains unchanged even for long propagation distances.

Superluminous drift

The asymptotic evolution of the three-wave interaction seems strongly related to the initial Stokes pulse width. The fully developed solitary and chaotic patterns presented in Figs. 1 and 5 correspond, respectively, to an initial wavefront slope $k=0.35$ and 18. We also investigate intermediate values. Figure 7 illustrates the evolution of the three waves for $k=0.75$, all other parameters being the same as in Figs. 1 and 5. The first stage of the interaction follows a scenario similar to that in Fig. 5 and the inertial instability appears ($t\cong 300$). Nevertheless, the overall Stokes energy is now sufficient to deplete noticeably the pump. The asymmetric

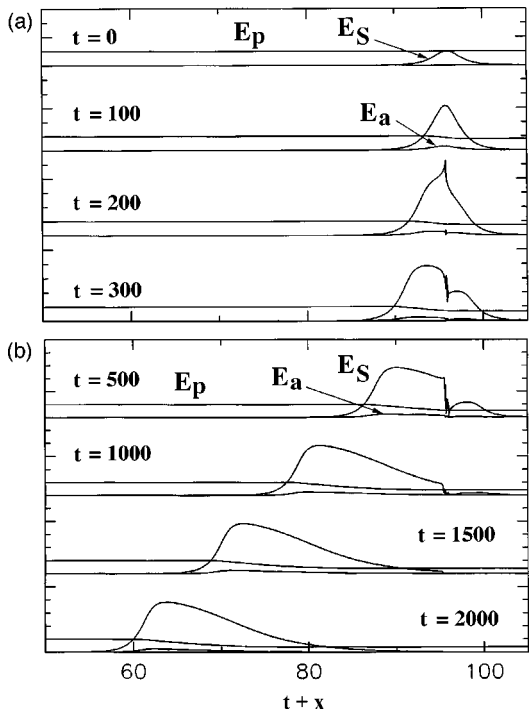

FIG. 7. Same as Figs. 1 and 5, but with an intermediary initial pulse ($k=0.75$): (a) onset of the inertial instability and (b) the superluminous front emerges from the chaotic dynamics and a solitary-wave attractor self-structures.

amplification process can thus happen: The leading front of the Stokes pulse follows a strong amplification to the detriment of the trailing edge where the *depleted pump is unsufficient to sustain the interaction*. Therefore, the inertial instability cannot fully develop and is relegated to the trailing edge of the pulse, while the wave front asymptotically reaches a steady solitary attractor propagating with a constant superluminous velocity.

In summary, due to its superluminous nature, the regular part of the three-wave structure drifts away from its chaotic part, which propagates at the luminous velocity. This idea is the same as for the separation of a defect whose characteristic time shorter than the width of the solitary structure allows a decoupled evolution (Fig. 2). The chaotic behavior presented in Fig. 5 is also characterized by a short time scale and similarly slides on the pulse tail at the luminous velocity to be damped in a finite time.

IV. ASYMPTOTIC ANALYSIS

So far we have qualitatively established that a variation of the initial condition, such as the width of the injected Stokes pulse or the pump intensity, drastically affects the spatiotemporal evolution of the three-wave interaction and that the velocity of the structure has a key role in its asymptotic behavior. The problem is now to find a quantitative criterion to describe the *selection* between the solitary and chaotic behaviors. One parameter that seems to play a fundamental role is the growth rate of the inertial instability. Also relevant is the *velocity* of the leading front of the Stokes field, which can be understood as the growth rate of the SRS convective instability.

A. Velocity: A relevant parameter

Brillouin and Sommerfeld define the *signal* and *front* velocities at which the half-maximum wave amplitude and the leading front of a wave packet would move, respectively [31]; the former is of interest to describe the ''luminous'' instability discussed above, while the latter characterizes the behavior of the evading ''superluminous'' part of the pulse. Thereafter, V will denote the front velocity. In the case of a solitary structure, both are equal to the *group* velocity at which the peak of the pulse would move, but generally not to the *energy* velocity [28].

A fundamental difference distinguishes the solitary solutions reported in classes (i) and (ii) of Sec. I, which result from a generalized NLS problem, from the characteristic solutions of the resonant three-wave problem reported in class (iii). It is straightforward that any solution u of the NLS equation

$$iu_x=\tfrac{1}{2}u_{tt}+|u|^2u \tag{3}$$

satisfies the gauge transformation

$$u(x,t-x/V)=u(x,t)\exp[i(x/2V^2+t/V)]. \tag{4}$$

This means that the search for solitary-wave behavior can be limited to the luminous velocity ($V=1$) case because ''moving'' solutions ($V\neq 1$) are derived from luminous ones through the transformation (4) [6]. We checked it even in complex representations such as the standard model of SRS. Therefore, a given solitary solution of a NLS problem, characterized, for instance, by the pulse width, can travel at any velocity, which is thus irrelevant.

The situation is completely different if one considers the pure three-wave resonant interaction ($\rho=0$, $\kappa=0$) which *breaks the existence of the gauge transformation*, the shape of the solitary wave being thus intimately related to its velocity [13,26]. The inertial model presents the ingredients of both NLS and three-wave problems. The velocity of the solitary wave thus becomes a relevant parameter even in dispersive propagation media.

B. Kolmogorov-Petrovskii-Piskunov procedure: Front velocity selection

When a physical system presents an instability, it is important to understand how it will evolve for long interaction times and then how the nonlinear stage of the interaction might saturate the instability. This problem has been discussed by Kolmogorov, Petrovskii, and Piskunov in the context of nonlinear diffusion problems [18]. The Kolmogorov-Petrovskii-Piskunov (KPP) method allows us to determine the asymptotic velocity of a front, when the transient have died out, through a linear analysis. Of particular interest for nonintegrable equations, it has been successfully applied to the pure dissipative three-wave interaction [20]. Above the SRS threshold, the Stokes wave is unstable, exponentially growing in the linear parametric regime [$E_p(x,t)=1$]. When the instability is saturated by depletion of the pump, a solitonlike structure can appear, as discussed above. The KPP asymptotic procedure then allows us to determine *ab initio* the front velocity in the linear parametric regime since the leading edge of the Stokes envelope always remains, by construction, in the linear undepleted pump regime. If and when a solitary regime is reached, this value is necessarily the velocity of the whole structure. Note that *the KPP procedure describes only the leading front of the Stokes field* and gives no information on the inertial instability that may arise in the body of the pulse.

Assuming an undepleted pump wave ($E_p=1$) and considering only the low-amplitude region where the nonlinear Raman and Kerr processes can be linearized, Eqs. (1) can be written

$$(\partial_t-\partial_x+i\rho\partial_{tt}+\mu_S-2i\kappa)(\partial_t+\mu_a)E_{S,a}=E_{S,a}. \tag{5}$$

The solution of this linear problem may be expressed as

$$E_S(x,t)=\int_C \tilde{E}_S(k)\exp[\gamma(k)t]\exp(kx)dk, \tag{6}$$

where k is complex and $\tilde{E}_S(k)$ is the Fourier transform of the initial Stokes field; $\gamma=\gamma(k)$ is obtained through the complex dispersion relation that characterizes the linear problem [$E_S\propto\exp(\gamma t+kx)$]:

$$(\gamma-k-2i\kappa+i\rho\gamma^2+\mu_S)(\gamma+\mu_a)=1. \tag{7}$$

Looking for traveling-wave solutions with velocity V [$\eta=x+Vt$, $\nu=t$], we write

$$E_S(\eta,\nu)=\int_C \tilde{E}_S(k)\exp[\gamma(k)-kV]\nu\ \exp(k\eta)dk. \tag{8}$$

This linear solution holds for long interaction times and gives the asymptotic velocity of the pulse wave front. The initial Stokes envelope has an exponential leading front and the function $\tilde{E}_S(k)$ has a pole for $k=k_0$. In fact, as a result of the three-wave parametric instability, the asymptotic wave-front structure grows exponentially. On the other hand, the function $f(k)=\gamma(k)-kV$ has a saddle point and the integral (8) can be calculated by the steepest descent method; the competing contributions of the pole and the saddle point are described in detail in Ref. [26]. It can be shown that the saddle point is the dominant contribution only for extremely short initial Stokes pulses (typically in the femtosecond range) where the slowly varying envelope approximation is violated and the present analysis is irrelevant. Then, for situations of physical interest for the inertial model, the integral is always dominated by the contribution of the pole of the function $\tilde{E}_S(k)$. The computation of Eq. (8) then reads

$$E_S(\eta,\nu)\propto\tilde{E}_S(k=k_0)\exp[\gamma(k_0)-k_0V]\nu\ \exp(k_0\eta). \tag{9}$$

It describes the asymptotic behavior (large ν) of the leading front of the Stokes envelope where the parametric approximation is always valid ($E_p=1$). As discussed before (Fig. 3), the phases are *not stationary* in the moving reference frame of velocity V, even when the superluminous attractor is already attained. Therefore, the steady-state condition of the solution (9) holds only for the amplitude $|E_S|$ and reads

$$V^*(k_0)=\frac{\mathrm{Re}[\gamma(k_0)]}{\mathrm{Re}(k_0)} \tag{10}$$

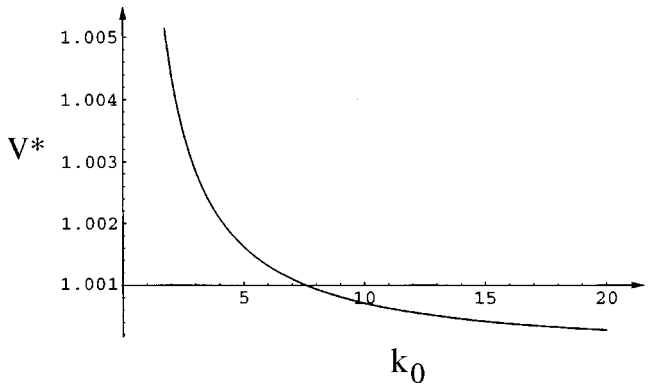

FIG. 8. Velocity V^* vs wave-front slope k_0 evaluated from Eq. (10). The steeper fronts travel more slowly than the smooth ones.

[whereas the phase velocity is $V_\phi = \mathrm{Im}\,\gamma/\mathrm{Im}\,k$ and the group velocity $V_g = \partial(\mathrm{Im}\,\gamma)/\partial(\mathrm{Im}\,k)$]. The front velocity V acts as a stabilizing parameter in Eq. (9): $V < V^*$ corresponds to an exponentially growing pulse and $V > V^*$ corresponds to a damped solution. Relation (10) thus defines a *neutral velocity*, for which the leading edge of the traveling wave neither grows nor decays in an amplifying medium (this quantity, although unusual in optics, is useful in nonlinear diffusion problems [21]).

Thus, whenever a steady regime is attained, the velocity of the three-wave solitary structure must be exactly V^*, which in turn is uniquely determined by the initial wave-front slope k_0 of the Stokes pulse. For a given set of parameters $(\mu_{S,a}, \rho, \kappa)$ the system is able to self-structure into a continuous family of dissipative structures characterized by the wave-front slope k_0 and the corresponding neutral velocity $V^*(k_0)$. If we neglect the group velocity dispersion ($\rho = 0$), we can generalize the expression obtained in Ref. [26] for the pure three-wave resonant model and derive an explicit analytical solution for V^* accounting for the optical Kerr effect:

$$V^*(k) = \frac{k_r - \mu_a - \mu_S + \Gamma}{k_r}, \tag{11}$$

where

$$\Gamma = \sqrt{2 + \tfrac{1}{2}\theta^2 - 2\kappa^2 + \tfrac{1}{2}\sqrt{[4(1-\kappa^2) + \theta^2]^2 + 16\kappa^2\theta^2}},$$

$$\theta = k_r + \mu_a - \mu_S .$$

A formal calculation gives a much more complicated expression of V^* when $\rho \neq 0$; we plot in Fig. 8 V^* versus k_0 for the same value of ρ as in Figs. 1 ($k_0 = 0.35$) and 7 ($k_0 = 0.75$). V^* has also been evaluated numerically for a number of realizations. The discrepancy $(V^*_{\mathrm{theor}} - V^*_{\mathrm{num}})/V^*_{\mathrm{num}}$ between the numerical and theoretical [Eq. (10)] values of V^* was always lower than 0.1%. The *steepest* front (large k_0) travels *more slowly* than the smooth front. This is a generic result, also found for the amplitude or Swift-Hohenberg equations [22]; however, in this last case, only the steepest front is stable since the initial condition is spatially bounded [26].

Neutral velocity of the chaotic structure

Even if the whole nonlinear solitary structure reaches the asymptotic steady state only after a long transient (Figs. 1 and 7), the KPP procedure assumes that the pulse wave front travels at the velocity $V^*(k_0)$ from the very beginning of the interaction if its initial shape is exponential, which is true even when the body of the pulse exhibits a chaotic evolution. Therefore, the KPP method always allows us to determine V^*, *even in the chaotic case*. We see here its discriminating role: For a short initial Stokes pulse (large k_0), $V^*(k_0)$ *is too small for the structure to drift away from the chaotic area*. It is thus crucial to evaluate the growth rate of the inertial instability in order to compare it to $V^* - 1$ and determine the long-term evolution of the three-wave interaction.

V. INERTIAL INSTABILITY

In this section we thus focus our attention on the instability that arises on the top of the Stokes pulse as discussed in Sec. III B. We investigate the nature of this kind of instability, which is intimately related to the combined actions of the optical Kerr effect and the noninstantaneous response of the propagation medium.

The stability analysis is carried out following the usual procedure outlined in Ref. [9] for the modulational instability. The numerical simulation reported in Figs. 5 and 6 shows that the modulus and the phase of the pump wave remains constant as the Stokes field develops the instability. This approximation holds even for large propagation distances; it allows us to set $E_p(x,t) = 1$ in the whole interaction range. Equations (1) then take the simplified form

$$[(1 + 2i\alpha\mu_a)\partial_\tau + \mu_a][\partial_\xi + i\rho\partial_{\tau\tau} + \mu_S]E_S = E_S + i\kappa[(1 + 2i\alpha\mu_a)\partial_\tau + \mu_a][|E_S|^2 + 2]E_S, \tag{12}$$

where $\xi = -x$ and $\tau = x + t$ still are the retarded variables. Equation (12) describes the propagation of the Stokes field in the *linear Raman regime* in the presence of the noninstantaneous response of the medium, group velocity dispersion, and Kerr nonlinearity [whereas in Eq. (5) both Raman and Kerr processes were linearized]. In order to get more physical insight, we will take into account only a *minimum* set of physical ingredients and neglect the amplification of the Stokes envelope; this supposes that the Stokes envelope reaches a quasicontinuous level (in Fig. 5 $E_S \cong 1.8$ at $t = 400$), conserved from then on. We therefore assume that $\mu_a\mu_S = 1$ and write

$$\partial_\xi E_S = -i\chi\partial_{\tau\tau}E_S - (1 + i\beta)[\partial_{\tau\xi} + i\chi\partial_{\tau\tau\tau} + \partial_\tau]E_S + i\eta[1 + (1 + i\beta)\partial_\tau][|E_S|^2 + 2]E_S, \tag{13}$$

where the space and time variables have been normalized ($\tau\mu \to \tau$, $\xi/\mu \to \xi$) and $\eta = \kappa\mu_a$, $\chi = \rho\mu_a^3$, and $\beta = 2\alpha\mu_a$. In the stationary case, Eq. (13) reduces to

$$\partial_\xi E_{S_0} = i\eta[|E_{S_0}|^2 + 2]E_{S_0}, \tag{14}$$

whose solution is given by

$$E_{S_0}(\xi) = q\ \exp[i\eta(q^2 + 2)\xi], \tag{15}$$

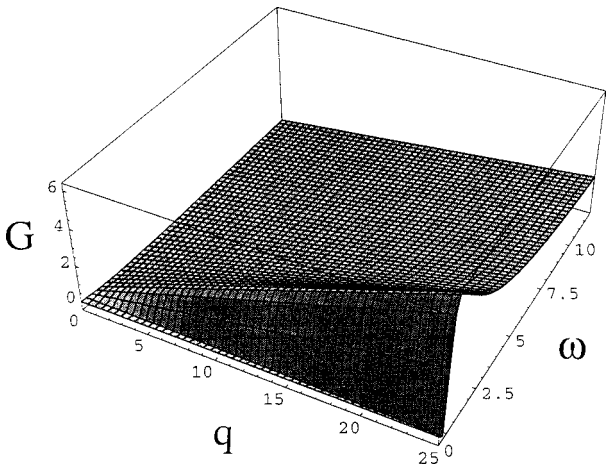

FIG. 9. Inertial instability growth rate vs modulational perturbation ω and Stokes amplitude q (analytical, $\rho=\chi=0$).

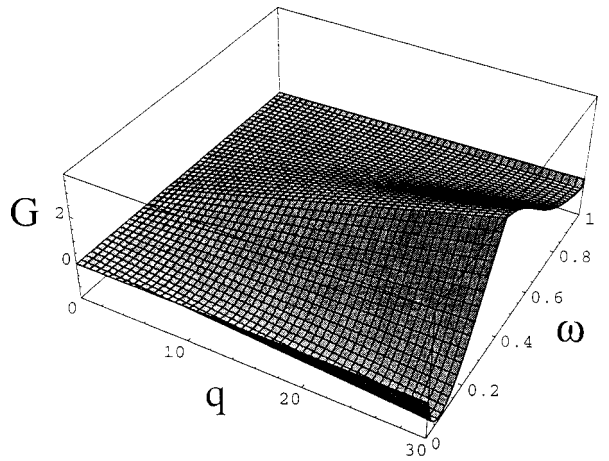

FIG. 10. Same as Fig. 9, but in the presence of normal group velocity dispersion.

where $q=E_{S_0}(\xi=0)$. We will now consider the evolution of the perturbation a defined as $E_S=E_{S_0}(\xi)+a(\xi,\tau)$; linearizing Eq. (13) with respect to a yields

$$\partial_\xi a=-i\chi a_{\tau\tau}-(1+i\beta)[\partial_{\tau\xi}+i\chi\partial_{\tau\tau\tau}+\partial_\tau]a + i\eta[ma+E_{S_0}^2a^*+(1+i\beta)(m\partial_\tau a+E_{S_0}^2\partial_\tau a^*)], \tag{16}$$

where $m=2(q^2+1)$. In order to avoid the $E_{S_0}^2$ terms we use the variable $d(\xi,\tau)=a(\xi,\tau)\exp[i\eta(q^2+2)\xi]$. Dividing $d(\xi,\tau)$ into its real and imaginary parts ($d=u+iv$) and considering the usual *ansatz* $d=d_0\exp(\lambda\xi+i\omega\tau)$, we get the dispersion relation

$$\{i\omega\beta(\lambda+1)-[2\eta q^2+\chi\omega^2](1+i\omega)\} \times[\chi\omega^2(1+i\omega)-i\beta\omega(\lambda+1)] =[\lambda(1+i\omega)+i\omega+i\omega^3\beta\chi] \times[\lambda(1+i\omega)+i\omega+i\omega\beta(\chi\omega^2+2\eta q^2)]. \tag{17}$$

The stationary solution (15) is unstable with respect to a perturbation of frequency ω whenever $\lambda(\omega)$ has a positive real part. The growth rate of the inertial instability $G=\mathrm{Re}\,\lambda$ is a symmetric function of the sideband detuning ω. Figure 9 represents the dependence of G on ω and the Stokes amplitude q in the absence of the group velocity dispersion ($\chi=0$); the other parameters are those used in all previous simulations. Below a cutoff frequency $\omega_{\max}$, the instability occurs without threshold for any q. The potentially unstable frequency band enlarges as the Stokes amplitude increases. The maximum growth rate $G_{\max}$ is also an increasing function of q and of the cw pump level E_0. The stationary solution is then unstable *even in the absence of the group velocity dispersion*.

We plot in Fig. 10 the instability growth rate G in the presence of the same positive dispersion as in the numerical simulations. Its main feature is to introduce a lower cutoff frequency $\omega_{\min}$, below which the instability is quenched. The noninstantaneous response of the medium then destabilizes the stationary solution *even in the normal dispersion regime* where conventional modulational instability does not occur. The growth rate G decreases as the relative weight of dispersion and inertial SRS increases.

The peak gain $G_{\max}$ is obtained for $\omega_0\cong 70$ in units of time $(KE_0)^{-1}$ corresponding to the normalization adopted in Eqs. (1) and in the numerical simulations. Therefore, the characteristic time scale of the instability ω_0^{-1} is much smaller than the width t_0 of the Stokes pulse ($\omega_0^{-1}\cong t_0/20$ in Fig. 5). This point justifies *a posteriori* the assumption of a stationary Stokes wave, which allowed our stability analysis.

This analysis gives information on the nature of the instability but does not describe the long-term evolution of the interaction that proved to be chaotic in some cases [2]. Nevertheless, it is worth noting that its time scale ω_0^{-1} fits fairly well the typical time scale of chaotic dynamics. This suggests that further insight might be obtained by means of a modal truncation of Eq. (12) to a finite number of harmonic components [32].

VI. DISCUSSION

The analytical tools developed in Secs. IV and V now allow us to compare the relative weight of the Raman and inertial instabilities. As expected, the ratio $(V^*-1)/G$ determines the asymptotic evolution of the three-wave interaction, G being evaluated in units of time $(KE_0)^{-1}$ [normalization adopted in Eqs. (1)]. When $G>V^*-1$ the inertial instability overcomes the Raman instability and the interaction evolves asymptotically toward a chaotic regime (in Fig. 5 $q\cong 1.8$, $G=4\times10^{-3}$, and $V^*-1=8.5\times10^{-5}$). In the opposite case the large velocity of the leading front is responsible for pump depletion, which freezes the inertial instability (in Fig. 7 $q\cong 2.5$, $G=6\times10^{-3}$, and $V^*-1=17\times10^{-3}$).

Thus the asymptotic evolution of a given initial condition is fully determined and predictable through a linear analysis *ab initio*, in very good agreement with the nonlinear numerical simulations. We verified that the KPP assertion, although rarely stated explicitly in nonlinear optics, still holds in the rather complex case of interest for stimulated Raman process in fibers, namely, for the strong three-wave interaction in the presence of the optical Kerr effect and chromatic dispersion. Here it means that the particular front slope corresponding to the neutral velocity V^* is selected from the very beginning

of the interaction and remains the front velocity of the whole structure up to asymptotic times. Moreover, we could extend the predictive power of this assertion by comparing V^*-1 to the gain G of the inertial instability, which has no threshold and is also active from the beginning.

The transition from the chaotic to solitonlike structures might be observed in a typical backward amplification experiment. For a typical fiber (effective area approximately equal to 100 μm^2 at $\lambda=1.32$ μm), the required continuous pump power, quite strong but still acceptable, is around 2 W for a length of 300 m. A subpicosecond sech-like signal should break down in a very irregular, poorly amplified output pulse, whose erratic shape would be very sensitive to the initial conditions and vary from one realization to another. On the other hand, longer signals, typically 10 ps and above, should yield solitary-wave behaviors and very repetitive outputs after an efficient amplification.

VII. CONCLUSION

In summary, we have investigated the dynamics of the SRS process in the frame of the inertial model. We have presented a class of dissipative coherent three-wave solitary structures that arise through a balance between three distinct physical processes: the stimulated Raman scattering, taking into account the noninstantaneous material response, the optical Kerr effect, and the dispersive effect. The three-wave resonant process breaks the gauge transformation specific to the NLS class of equations. The velocity of the solitary wave then plays a key role and governs the long-term evolution of the three-wave interaction, through an original evasion process, luminous defects or chaotic tails being left behind by the solitary structure whenever its superluminous velocity is sufficient to take over the instability growth. Besides this solitonlike motion, the Kerr process coupled to the noninstantaneous response of the medium yields a different kind of inertial instability that evolves asymptotically towards a chaotic behavior.

APPENDIX A

Representing the complex fields E_i by their real amplitudes and phases $[E_i=A_i\exp(i\phi_i)]$ and considering the phase mismatch $\Phi=\phi_p-(\phi_S+\phi_a)$, we can rewrite system (1) as

$$(\partial_t+\partial_x)A_p-2\rho\partial_t A_p\partial_t\phi_p-\rho A_p\partial_{tt}\phi_p-\mu_p A_p=-A_S A_a\cos\Phi, \tag{A1a}$$

$$(\partial_t-\partial_x)A_S-2\rho\partial_t A_S\partial_t\phi_S-\rho A_S\partial_{tt}\phi_S-\mu_S A_S=A_p A_a\cos\Phi, \tag{A1b}$$

$$\partial_t A_a-2\alpha\mu_a A_a\partial_t\phi_a+\mu_a A_a=A_p A_S\cos\Phi, \tag{A1c}$$

$$A_p(\partial_t+\partial_x)\phi_p+\rho\partial_{tt}A_p-\rho A_p(\partial_t\phi_p)^2=A_S A_a\sin\Phi+\kappa(A_p^2+2A_S^2)A_p, \tag{A1d}$$

$$A_S(\partial_t-\partial_x)\phi_S+\rho\partial_{tt}A_S-\rho A_S(\partial_t\phi_S)^2=A_p A_a\sin\Phi+\kappa(A_S^2+2A_p^2)A_S, \tag{A1e}$$

$$A_a\partial_t\phi_a+2\alpha\mu_a\partial_t A_a=A_p A_S\sin\Phi. \tag{A1f}$$

The amplitudes and the phases are resonantly coupled through the phase mismatch Φ. The system generally tends to maximize the pump-to-Stokes conversion efficiency and thus to select $\Phi=0$ for which the SRS gain is *maximum*. $\Phi=\pi$ corresponds to reverse energy transfer from the Stokes to the pump wave.

APPENDIX B

Starting from Eqs. (1), we multiply each equation by the corresponding complex conjugate field, yielding

$$(2\partial_\tau-\partial_\xi+2\mu_p)|E_p|^2=-E_S E_a E_p^*-i\rho E_p^*\partial_{\tau\tau}E_p+\text{c.c.}, \tag{B1a}$$

$$(\partial_\xi+2\mu_S)|E_S|^2=E_p E_a^* E_S^*-i\rho E_S^*\partial_{\tau\tau}E_S+\text{c.c.}, \tag{B1b}$$

$$(\partial_\tau+2\mu_a)|E_a|^2=E_p E_a^* E_S^*-2i\alpha\mu_a E_a\partial_\tau E_a^*-i\alpha E_a\partial_{\tau\tau}E_a^*+\text{c.c.}, \tag{B1c}$$

where $\xi=-x$ and $\tau=t+x$ are the retarded variables and c.c. denotes the complex conjugate. The energies of the material and Stokes fields are proportional to

$$W_{S,a}=\int_{-\infty}^{+\infty}|E_{S,a}|^2 d\tau. \tag{B2}$$

Integrating in time the above expressions and assuming the Stokes and material envelopes to be localized $[E_{S,a}(\tau\to\pm\infty)=0]$ yield

$$\partial_\xi W_S=2\mu_a W_a-2\mu_S W_S+4i\alpha\mu_a\int_{-\infty}^{+\infty}E_a^*\partial_\tau E_a d\tau. \tag{B3}$$

When the three fields reach an asymptotic steady state, the integrated Stokes energy becomes constant and Eq. (B3) yields the expression of the invariant

$$I=-\mu_S W_S+\mu_a W_a+2i\alpha\mu_a\int_{-\infty}^{+\infty}E_a^*\partial_\tau E_a d\tau. \tag{B4}$$

Note that $\int_{-\infty}^{+\infty}E_a^*\partial_\tau E_a d\tau=-\int_{-\infty}^{+\infty}\partial\tau E_a^* E_a d\tau$; therefore, $\int_{-\infty}^{+\infty}E_a^*\partial_\tau E_a d\tau$ is a pure imaginary number.

[1] C. Headley III and G. P. Agrawal, J. Opt. Soc. Am. B **13**, 2170 (1996).

[2] A. Picozzi, C. Montes, J. Botineau, and E. Picholle, J. Opt. Soc. Am. B **15**, 1309 (1998).

[3] J. P. Gordon, Opt. Lett. **11**, 662 (1986).

[4] J. Herrmann and A. Nazarkin, Opt. Lett. **19**, 2065 (1994); Phys. Rev. E **53**, 6492 (1996).

[5] Y. S. Kivshar, Phys. Rev. A **42**, 1757 (1990).

[6] Y. S. Kivshar and S. K. Turitsyn, Phys. Rev. A **47**, R3502 (1993).

[7] G. P. Agrawal and C. Headley III, Phys. Rev. A **46**, 1573 (1992).
[8] M. Gedalin, T. C. Scott, and Y. B. Band, Phys. Rev. Lett. **78**, 448 (1997).
[9] G. P. Agrawal, *Nonlinear Fiber Optics*, 2nd ed. (Academic, San Diego, 1995).
[10] D. N. Christodoulides, Opt. Commun. **86**, 431 (1991).
[11] R. I. Joseph and D. N. Christodoulides, Opt. Lett. **17**, 1101 (1992).
[12] W. Kaiser and M. Maier, in *Laser Handbook*, edited by F. T. Arecchi and E. O. Schulz-Dubois (North-Holland, Amsterdam, 1972), p. 1077.
[13] D. J. Kaup, A. Reiman, and A. Bers, Rev. Mod. Phys. **51**, 275 (1979).
[14] C. R. Menyuk, Phys. Rev. Lett. **62**, 2937 (1989); C. R. Menyuk, D. Levi, and P. Winternitz, *ibid.* **69**, 3048 (1992).
[15] D. J. Kaup, Physica D **6**, 143 (1983); H. Steudel, *ibid.* **6**, 155 (1983).
[16] K. Drühl, R. G. Wenzel, and J. L. Carlsten, Phys. Rev. Lett. **51**, 1171 (1983).
[17] A. V. Buryak, Y. S. Kivshar, and S. Trillo, Phys. Rev. Lett. **77**, 5210 (1996); A. V. Buryak and Y. S. Kivshar, *ibid.* **78**, 3286 (1997); R. A. Fuerst, D.-M. Baboiu, B. Lawrence, W. Torruellas, G. I. Stegman, S. Trillo, and S. Wabnitz, *ibid.* **78**, 2756 (1997).
[18] V. G. Kolmogorov, I. G. Petrovskii, and N. S. Piskunov, Bull. Moscow State University, Math. Mechanics **1**, 1 (1937).
[19] V. G. Kamenskii and S. V. Manakov, JETP Lett. **45**, 638 (1987); S. V. Manakov and V. G. Kamensky, in *Nonlinear Evolution Equations: Integrability and Spectral Methods*, edited by A. Degasperis, A. P. Fordy, and M. Lakshmanan (Manchester University Press, Manchester, 1990), p. 477.
[20] C. Montes, A. Mikhailov, A. Picozzi, and F. Ginovart, Phys. Rev. E **55**, 1086 (1997).
[21] G. Dee and J. S. Langer, Phys. Rev. Lett. **50**, 383 (1983).
[22] W. van Saarloos, Phys. Rev. Lett. **58**, 2571 (1987); G. Dee and W. van Saarloos, *ibid.* **60**, 2641 (1988).
[23] K. J. Blow and D. Wood, IEEE J. Quantum Electron. **QE-25**, 2665 (1989).
[24] C. C. Chow and A. Bers, Phys. Rev. A **47**, 5144 (1993).
[25] E. Picholle, C. Montes, C. Leycuras, O. Legrand, and J. Botineau, Phys. Rev. Lett. **66**, 1454 (1991).
[26] C. Montes, A. Picozzi, and D. Bahloul, Phys. Rev. E **55**, 1092 (1997).
[27] C. C. Chow, Physica D **81**, 237 (1995).
[28] R. Y. Chiao, in *Amazing Light*, edited by R. Y. Chiao (Springer, New York, 1996).
[29] C. Montes, E. Picholle, J. Botineau, O. Legrand, and C. Leycuras, in *Nonlinear Coherent Structures in Physics and Biology*, edited by M. Remoissenet and M. Peyrard, Lecture Notes in Physics Vol. 393 (Springer-Verlag, Berlin, 1991), p. 44.
[30] E. V. Vanin, A. I. Korytin, A. M. Sergeev, D. Anderson, M. Lisak, and L. Vazquez, Phys. Rev. A **49**, 2806 (1994).
[31] L. Brillouin, *Wave Propagation and Group Velocity* (Academic, New York, 1960).
[32] M. Haelterman, S. Trillo, and S. Wabnitz, Phys. Rev. A **47**, 2344 (1993).